Nanoscale Longitudinal Normal Strain Behavior of Si_3N_4-to-ANSI 304L Brazed Joints under Pure Bending Condition

D. W. Seo and J. K. Lim

Abstract

To combine the mechanical advantages of ceramics with those of metals, one often uses both materials within one composite component. But, as known, they have different material properties and fracture behaviors. In this study, a four-point bending test is carried out on Si_3N_4 joined to ANSI 304L stainless steel with a Ti-Ag-Cu filler and a Cu interlayer at room temperature to evaluate their longitudinal strain behaviors. And, to detect localized strain, a couple of strain gages are pasted near the joint interfaces of the ceramic and metal sides. The normal strain rates are varied from 3.33×10^{-5} to 3.33×10^{-1} s^{-1}. Within this range, the experimental results showed that the four-point bending strength and the deflection of the interlayer increased with increasing the strain rate.

Key Words: Si_3N_4/ANSI 304L, Four-point bending, Residual strain, Strain rate, Brazed joints.

Nomenclature

α	Thermal expansion coefficient
δ_i	Downward deflection at the inner supports in four-point bending
δ_m	Downward deflection at the midpoint of the beam
ε_x	Strain in the longitudinal direction
$\varepsilon_{x,m}$	Longitudinal normal strain at the outer fiber of the midpoint of the beam
θ	Angle
ρ	Radius of curvature
σ_{4p}	Four-point bending strength
υ	Poisson's ratio
E	Young's modulus
h	Height of beam
l	Inner span of four-point bending test
L	Outer span of four-point bending test
M_x	Bending moment
P	Maximum load
t	Thickness of specimens
w	Width of specimens

D. W. Seo : Materials & Fracture Laboratory, Department of Mechanical Design, Chonbuk National University, Chonju, Korea

J. K. Lim : Department of Mechanical and Aerospace System Engineering, Chonbuk National University, Chonju, Korea

E-mail : jklim@chonbuk.ac.kr

1. Introduction

The introduction of ceramic-metal joining is important in the application of ceramics to the structural components. It could make the best use of the merit and make up for the demerit. The fracture strength of the ceramic/metal joint is, however, influenced by the residual stresses and the stress concentration (the singular stress field) caused by the difference between the thermal expansion coefficients and between the elastic moduli.[1] Many experimental studies have been conducted on the material

combinations and the joining method.[2~4] Some analytical studies on the thermal and residual stresses have been conducted.[1),5~8] And some experimental studies on the strength of the ceramic/metal joint have also been conducted.[9~11] To evaluate the fracture behavior of the ceramic/metal joint accurately, however, it is necessary to evaluate the longitudinal normal strain behavior at the brazed interfaces and the effect of strain rate on the strength of the joint.

In this study, four-point bending tests were conducted on Si_3N_4/ANSI 304L stainless steel joint specimens with various strain rates. To evaluate localized strains, a couple of strain gages were pasted near the joint interfaces at the Si_3N_4 and ANSI 304L sides. The longitudinal normal strain (elongation) behaviors with plastic and residual strain under pure bending condition are discussed on the basis of several experimental and theoretical results. The effect of strain rate is also discussed.

2. Relation of longitudinal normal strain to crosshead displacement

Let us consider the beam transversely loaded as the four-point bending test. Note that the middle portion *CD* (see Fig. 1) of the beam is free from shear force and that its bending moment M_x is uniform between *C* and *D* ; this condition is known as pure bending.

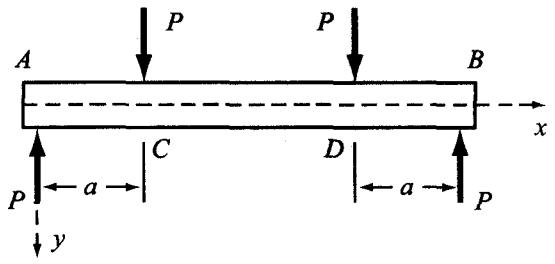

Fig. 1 Beam in four-point bending

To investigate the state of internal strain produced by pure bending, we shall assume that the beam obeys Hooke's law with the addition of several required assumptions : (1) linear-elastic stress-strain behavior, and (2) plane sections remaining plane after deformation, which combine to require a linear stress distribution. Then since the bending moment is uniform between *C* and *D*, it is reasonable to assume that the bending deformation will also be uniform ; that is, portion *CD* of the beam will take the form of a circular arc as shown Fig. 2. As a result of the deformation, the fibers on the convex side of the beam are elongated slightly while those on the concave side are shortened slightly.

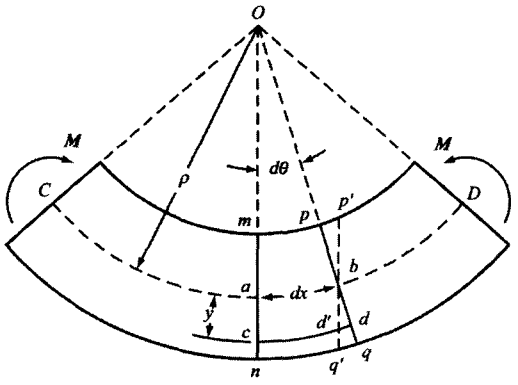

Fig. 2 Deformation of a beam in pure bending

In Fig. 2, we now draw, through point b on the neutral axis, a line $p'q'$ parallel to *mn* and indicating the original orientation of the cross-section *pq* before bending. From this construction, we see that segment cd' of any fiber at distance y from the neutral surface elongates by the amount $d'd = yd\theta$. Since its original length was $cd' = dx$, the corresponding strain is[11] :

$$\varepsilon_x = \frac{yd\theta}{dx} = \frac{y}{\rho} \tag{1}$$

where ε_x is the strain in the longitudinal (x) direction, and ρ is the radius of curvature. The downward deflection δ_m at the midpoint of the beam can be calculated now. Because the deflection curve is a circular arc, the deflection is :

$$\delta_m = \rho(1 - \cos d\theta) \tag{2}$$

For a nearly flat curve, we can assume that the distance between supports is equal to the length l of the beam (inner span). Therefore,

$$\sin d\theta = \frac{l}{2\rho} \tag{3}$$

Since $l/2\rho$ is a very small value and θ is a very small angle, we can consider following assumptions :

$$\sin d\theta \approx d\theta \qquad \cos d\theta \approx \frac{1-\theta^2}{2} \tag{4}$$

Now we substitute into equation (2) for the deflection and obtain :

$$\delta_m \approx \frac{\rho\theta^2}{2} = \frac{l^2}{8\rho} \tag{5}$$

Rearranging equation (5) and substituting into equation (1), we obtain :

$$\varepsilon_{x,m} = \frac{4h}{l^2}\delta_m \tag{6}$$

where $\varepsilon_{x,m}$ is the longitudinal normal strain at the outer fiber of the midpoint of the beam and the height of beam $h = 2y$. Considering a downward deflection δ_i at the inner supports in four-point bending, we can also lead to the following expression for strain at the midpoint :

$$\varepsilon_{x,m} = \frac{h(sL^2-4a^2)}{l^2(3L-2a)}\delta_i \tag{7}$$

where L and l are the distances between the outer and inner supports, respectively, and $a = (L\text{-}l)/2$. Now we can obtain the longitudinal normal strain at the outer fiber from the information of deflections at the midpoint or inner supports, that is, the displacements of the crosshead.

3. Experimental details

The pressureless-sintered Si_3N_4 and ANSI 304L austenitic stainless steel were joined by the active metal vacuum-brazing method. A copper sheet was used as the interlayer and Ti-Ag-Cu alloy (Cusil-ABA, WESGO Metals, USA) was used as the brazing filler metal. The material properties and the conditions of joining are listed in Tables 1 and 2, respectively.

Table 1 Mechanical properties

	Si_3N_4	ANSI 304L	Cu
E(GPa)	304	196	108
υ	0.24	0.30	0.33
α	3.0	17.3	17.7

E : Elastic modulus

υ : Poisson's ratio

α : Coefficient of thermal expansion

Table 2 Condition of joining

Brazing filler	Ti-Ag-Cu
Temperature	1073 - 1123K
Atmosphere	Vacuum, 1.3×10^{-3}Torr
Interlayer	Cu (thickness, 0.2mm)

The configuration and dimensions of the specimens are shown in Fig. 3 and 4. Si_3N_4 specimens were cut into 3×4×20mm bars. The bond surface of each bar, a 3×4mm face of the bar, was ground to an average surface roughness of about 0.5μm. Other faces of the bar were polished with fine mesh SiC abrasive paper and then ultrasonically cleaned in acetone. ANSI 304L specimens with the same dimensions as the Si_3N_4 specimens were prepared and the faces to be bonded were finished with a 1200 grit SiC abrasive paper and macro-etched to remove any oxide films. The thickness of the copper interlayer and Ti-Ag-Cu brazing filler were 0.25 - 0.30mm and 0.05 - 0.125mm respectively. The Si_3N_4/ANSI 304L stainless steel joint specimens without pre-crack for the four-point bending test are shown in Fig. 4. The four-point bending test procedures were conducted in accordance with the ASTM standard (1993). The interface was set at the midpoint of the span.

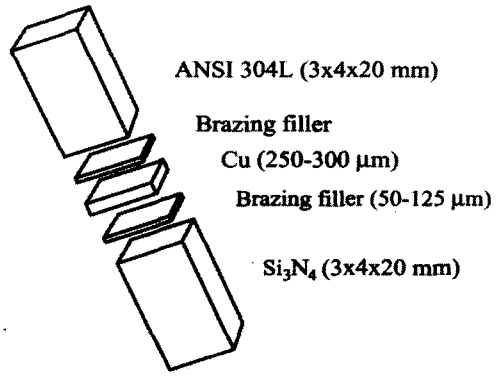

Fig. 3 Specimen configuration

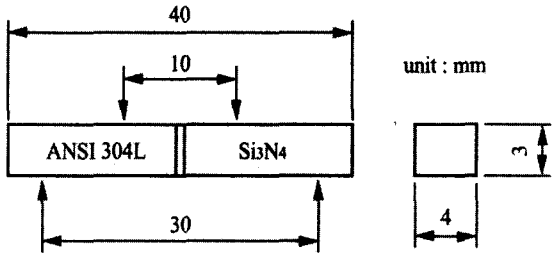

Fig. 4 Dimensions of four-point bending specimen

The test procedures were performed by hydraulic universal test machine, Instron model 8516 with 1-ton load cell. The outer span distance was 30mm and inner was 10mm. The nominal bending strength σ_{b4} ignoring the material discontinuity was calculated from the following equation (ASTM standard, 1993) :

$$\sigma_{b4} = \frac{3P(L-l)}{2bh^2} \quad (8)$$

where P is the maximum load (fracture load), L is the outer span, l is the inner span, b is the specimen width and h is the specimen height.

The test was carried out at various crosshead speeds (CHS), 0.005, 0.05, 0.5, 5 and 50mm/min, to evaluate the effect of strain rate on the strength of the joint at room temperature. To evaluate the strains that accompany the plastic deformation in localized areas at the edge of a beam, a couple of strain gages were pasted near the joint interfaces at the Si_3N_4 and ANSI 304L sides. The strain gage was pasted on lower side that applied tensile load and its gage length was 2mm.

4. Results and discussion

4.1 Effect of strain rate

The relations between the bending strength and the various crosshead speeds obtained by the four point bending tests conducted at room temperature are shown in Fig. 5, where the strength is plotted as a function of the logarithm of the crosshead speed. The curve in Fig. 5 shows a linear increase of the bending strength from CHS = 0.005mm/min up to CHS = 50 mm/min. This result is in reasonable agreement with other published works for Ti alloy and other metals.[12, 13] The specimens, tested at room temperature, were mainly fractured along the interfaces between the Cu interlayer and the metal side (ANSI 304L). The cracks initiated at the reaction layer of the metal-brazing filler, so the fracture behavior was similar to metals.

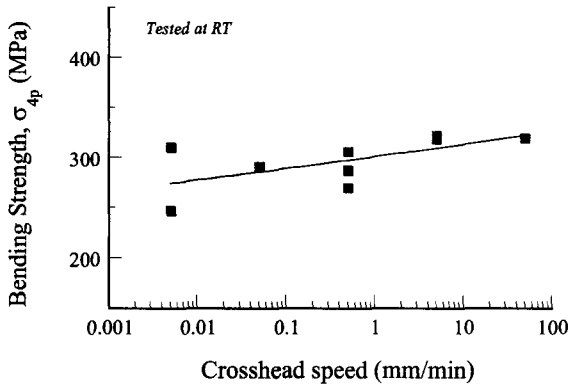

Fig. 5 4-point bending strength as a function of crosshead speed

The variation in the deflection of Cu interlayer, the center of specimen, is illustrated in Fig. 6 with various crosshead speeds. The deflection level of interlayer at maximum strength generally increased with increasing crosshead speed. This result might be influenced by increasing strength resulted from the high loading speed in the relatively high CHS region. The

downward flex of the specimens, namely, increased with increasing applied load.

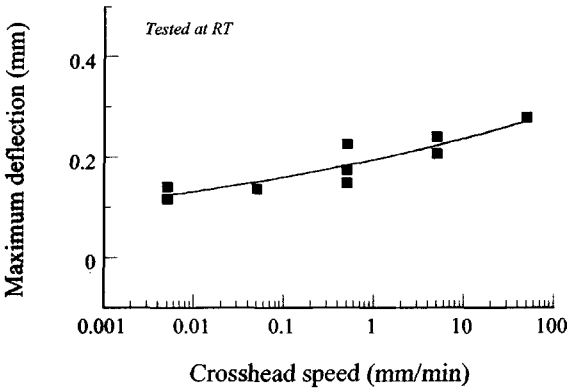

Fig. 6 Maximum deflection as a function of crosshead speed

The variation in the maximum localized strain with various crosshead speeds near the joint interfaces of the Si_3N_4 and ANSI 304L is illustrated in Fig. 7. This curves show the strains at maximum strength, that is, at fracture. The tensile load was applied to strain gages, perpendicular to ceramic/metal interface. The strain level of the metal side remained almost constant with increase in strain rate. But, the localized strain of the ceramic side showed a tendency that gradually increased with increasing strain rates. At relatively higher strain rates, the gap in the strain levels between the Si_3N_4 and ANSI 304L was small. This may be due to the high loading speed applied to specimens. The individual deformation seemed to be impossible because two materials were joined with brazing alloy and the high loading speed was applied. In the relatively lower strain rate region, the strain value of Si_3N_4 was almost zero, but the strain level of ANSI 304L was slightly increased because of characteristics of relatively ductile metal.

Fig. 8 shows the residual strains of the metal and ceramic, which remained after fracture, at various crosshead speeds. The residual strain value of metal is larger than ceramic. The residual strains of ANSI 304L ranged from 200×10^{-3} to 1000×10^{-3}nm and of Si_3N_4, from 5×10^{-3} to 20×10^{-3}nm. These behavior patterns are typical characteristics of metals and ceramics. The gap in residual strain levels between the Si_3N_4 and ANSI 304L gradually decreased with increasing strain rates.

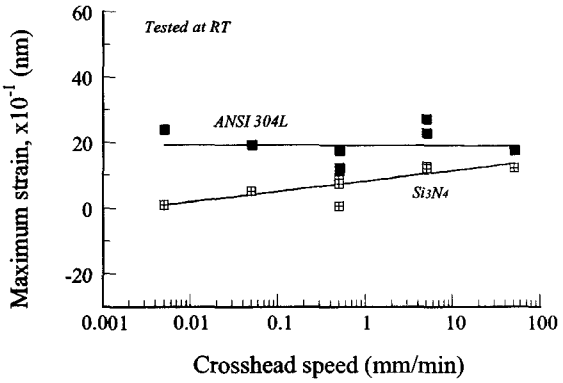

Fig. 7 Maximum strain as a function of crosshead speed

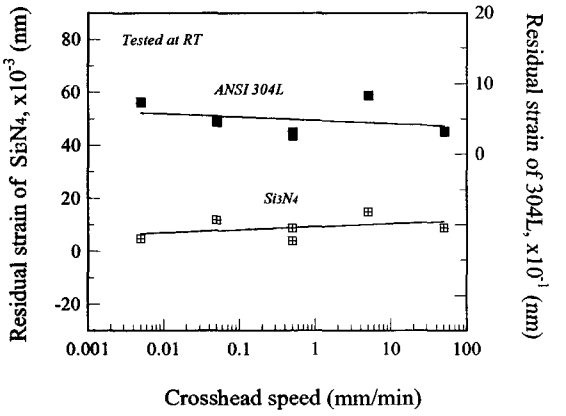

Fig. 8 Residual strain of metal and ceramic as a function of crosshead speed

4.2 Effect of temperature

The relations between the bending strength and the test temperature obtained from the four point bending tests at CHS = 0.5mm/min, are shown in Fig. 9. At the high test temperature region, from 100 to 500 ℃, the bending strengths gradually decreased with increasing test temperature. The specimens, tested at high temperatures, were mainly fractured along the interfaces between the Cu interlayer and the ceramic side (Si_3N_4). The cracks initiated at the reaction layer of the ceramic-brazing filler (Ti-reactions). As above

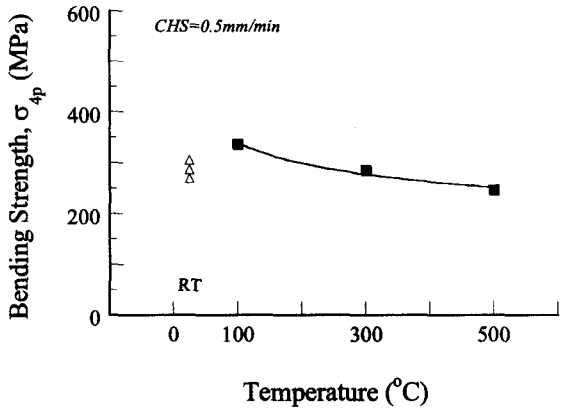

Fig. 9 4-Point bending strength as a function of test temperature

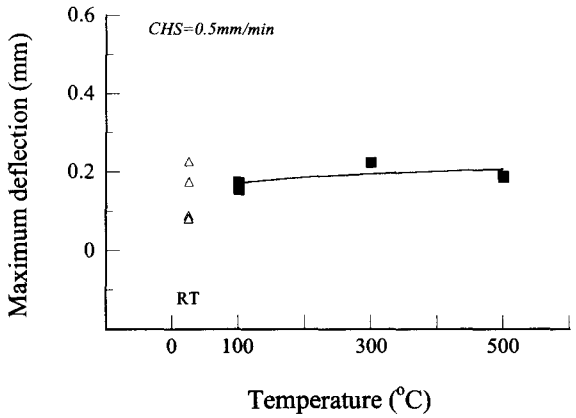

Fig. 10 Maximum deflection as a function of test temperature

mentioned, in the room temperature test, the crack progressed along the interface between Cu interlayer and ANSI 304L. But, at elevated temperatures, the weak point was changed to Cu/Si_3N_4 interface. It seems that the large difference of thermal expansion between metal (Cu) and ceramics (Si_3N_4) make to concentrate stress on the Cu/Si_3N_4 interface. The difference of thermal expansion between the two materials may have increased with increasing temperature, and the concentrated stress has increased. Because of the above reasons, the strength decreased with increasing temperature. The marks (Δ) that showed the results at RT are for comparison with the strength at room temperature.

The variation in the deflection of Cu interlayer, center of specimen, is illustrated in Fig. 10 with various test temperatures at CHS = 0.5mm/min. In the elevated temperature region, the result shows no significant change in the deflection. The values on this curve mean the deflections to fracture. Testing was started after their surrounding temperature became stable. From then on, the acquisition of deflection values was measured to failure. That is, the deflection of Cu affected by heating was not considered. Thus, the loading deflection level of Cu interlayer was low.

5. Conclusion

The longitudinal normal strain behaviors with plastic and residual strain under pure bending condition were discussed on the basis of several experimental and theoretical results. Four-point bending tests were conducted for Si_3N_4/ANSI 304L stainless steel joined specimens at various strain rates to evaluate localized strain behaviors. The results obtained are as follows.

The bending strengths linearly increased with increasing strain rate at room temperature. The cracks initiated at the reaction layer of the metal-brazing filler, so fracture behaviour was similar to metals. The downward deflection of Cu interlayer increased with increasing strain rate at room temperature, because of increasing strength with high loading speed. With the increase of strain rates at room temperature, the gaps in the strain and residual strain levels between the Si_3N_4 and ANSI 304L were gradually decreased, because two materials were joined with brazing alloy and high loading speed applied. The longitudinal normal strain at the outer fiber was easily obtained from the values of deflections at the midpoint or inner supports.

References

1. H. Kobayashi, Y. Arai, H. Nakamura, and T. Sato : Strength evaluation of ceramic-metal joints, *Mater. Sci. Eng.*, Vol. A143, (1991), pp. 91-102

2. A. H. Elsawy and M. F. Fahmy : Brazing of Si_3N_4 ceramic to copper, *J. Mater. Process. Tech.*, Vol. 77, (1998), pp. 266-272
3. R. A. Marks, D. R. Chapman, D. T. Danielson, and A. M. Glaeser : Joining of alumina via copper/ niobium/copper interlayers, *Acta Mater.*, Vol. 48, (2000), pp. 4425-4438
4. J. W. Park, P. F. Mendez, and T. W. Eagar : Strain energy distribution in ceramic-to-metal joints, *Acta Mater*, Vol. 50, (2002), pp. 883-899
5. T. W. Kim, H. S. Chang, and S. W. Park : Re-distribution of thermal residual stress in a brazed Si_3N_4/stainless steel joint using laminated interlayers, *J. Mater. Sci. Lett*, Vol. 20, (2001), pp. 973-976
6. S. B. Lee and J. H. Kim : Finite-element analysis and X-ray measurement of the residual stresses of ceramic/metal joints, *J. Mater. Process. Tech*, Vol. 67, (1997), pp. 167-172
7. D. Yoshikawa, A. Kikuchi, and T. Takahashi : Residual stress and phase transformation in the Y-PSZ/metal joints, *Mater. T. JIM.*, Vol. 37, No. 4 (1996), pp. 748-753
8. P. J. Yvon, B. Marty, and S. D. Peteves : Effects of the metal workpiece properties on the residual stresses in silicon nitride-metal brazed joints, *J. Mater. Res.*, Vol. 11, No. 12 (1996), pp. 3090-3098
9. J. H. Kim and Y. C. Yoo : Microstructure and bond strength of Ni-Cr steel/Si_3N_4 joint brazed with Ag-Cu-Zr alloy, *Mater. Sci. Technol.*, Vol. 14, (1998), pp. 352-356
10. R. Weiss and F. Sassani : Strength of friction welded ceramic-metal joints, *Mater. Sci. Technol.*, Vol. 14, (1998), pp. 554-560
11. J. M. Gere and S. P. Timoshenko : Mechanics of Materials, *PWS Publishing Company*, (1997), pp. 308
12. M. Jain, M. C. Chaturvedi, N. L. Richards, and N. C. Goel : Strain rate sensitivity effects with forming characteristics of superplastic Ti-6Al-4V, *Mater. Sci. Eng.*, Vol. A138, (1991), pp. 205-211
13. W. S. Lee and M. T. Lin : The effects of strain rate and temperature on the compressive deformation behaviour of Ti-6Al-4V alloy, *J. Mater. Process. Technol.*, Vol. 71, (1997), pp. 235-246